1992

Constructing Cl Surfaces of Arbitrary Topology Using Biquadratic and Bicubic Splines

Jörg Peters

Report Number:
92-070

CONSTRUCTING C1 SURFACES OF ARBITRARY TOPOLOGY USING BIQUADRATIC AND BICUBIC SPLINES

Jorg Peters

CSD-TR-92-070
September 15, 1992

Constructing C^1 surfaces of arbitrary topology using biquadratic and bicubic splines

by

Jörg Peters[†]
jorg@cs.purdue.edu

Key words: C^1 surface, vertex enclosure, reparametrization, corner cutting

Running title: Smooth biquadratic-bicubic surfaces

Version: Aug 25 92 **Date printed:** September 15, 1992

Submitted to: Designing fair curves and surfaces, N. Sapidis (ed.), May 15 1992

Abstract

Given a bivariate mesh of points, a C^1 surface of corresponding genus and connectedness is constructed. Most of the surface is parametrized by a biquadratic spline whose control points are obtained by refining the input mesh via corner cutting. The remaining mesh regions are parametrized by bicubic patches in Bernstein-Bézier form. The construction can be extended to rational patches and to interpolate at the vertices of the input mesh.

[†] Department of Computer Science, Purdue University, W-Lafayette IN 47907
Supported by NSF grant CCR-9211322

1. Introduction

Repeated corner cutting to smoothen a polytope is an intuitively appealing design paradigm. This paradigm is algorithmically realized by generalized subdivision. Given a bivariate input mesh[1], the algorithms of [Catmull and Clark '78], [Doo '78], [Loop '87], [Dyn, Levin and Liu '92] to name just a few, create at each stage a refined mesh of points by averaging neighboring points of the current mesh according to one or more weight patterns called masks. For properly chosen cut ratios, some regular meshes can be interpreted as control point meshes of box and tensor-product splines. However, only surfaces of genus one can be modeled with such regular meshes. And even then, local geometric considerations may call for an irregular mesh. Thus, general surface modeling requires irregular meshes and generalized subdivision schemes do not provide a parametrization of the corresponding limit surface. This not only makes it tricky to establish elementary properties like tangent plane continuity of the limit surface (see e.g. [Doo, Sabin 78], [Ball, Storry '86,'88,'89]), but is also a major obstacle for integrating these techniques with other CAGD representations.

Starting from analytic descriptions of surface pieces, called patches, a large number of surface constructions for meshes of arbitrary genus and connectedness have been derived (see e.g. [Gregory '90] for a survey). Predictably, the smooth joining of more than four patches at a common point and the dual problem of covering non quadrilateral mesh cells has been the central difficulty. A number of solutions have been suggested that either sacrifice the low degree of the surfaces (e.g. [Sarraga '87],[Hahn '89]) or depart from the standard tensor-product B-spline representation (e.g. [Gregory '74], [Loop, DeRose '90]). The central idea of the parametric approach is to reparametrize when crossing from one patch to the next. This shifts the focus from the geometric paradigm of subdivision to clever uses of the chain rule. For example G-spline spaces ([Sabin '83], [Goodman '88] and [Höllig, Mögerle '89]) are obtained by fixing the reparametrizations *a priori* dependent only on the connectedness of the patches but not on the geometric data. In order to match the data, large sparse linear systems in the patch coefficients have to be solved. This makes it tricky to reason about the shape of the resulting surface.

The algorithm to be detailed here reconciles the subdivision paradigm with the parametric approach. In an initial step, it refines a given open or closed bivaraiate mesh of arbitrary topology to give the surface its rough shape and separate irregular mesh regions. It then fits a biquadratic C^1 spline over the regular mesh regions and covers the remaining non quadrilateral cells with bicubic patches so that the resulting surface has a polynomial representation of *low* degree. Remarkably, the Bernstein-Bézier coefficients of the polynomial patches can be derived from the input mesh by applying a sequence of convolution masks; thus, in contrast to other parametrizations, no system of equations has to be solved to build the surface.

From an analytic point of view, the proposed and implemented bicubic tangent-plane continuous extension of the standard biquadratic tensor-product spline surface can be viewed as an alternative to rational blending schemes, S-patches and global methods. The approach differs from [Hahn '89] and [Höllig, Mögerle '89] and [Mögerle '92] in that the

[1] The mesh cells are isomorphic images of polygons but not necessarily planar. Therefore neither polyhedral mesh nor 1-skeleton is an appropriate name for the input mesh.

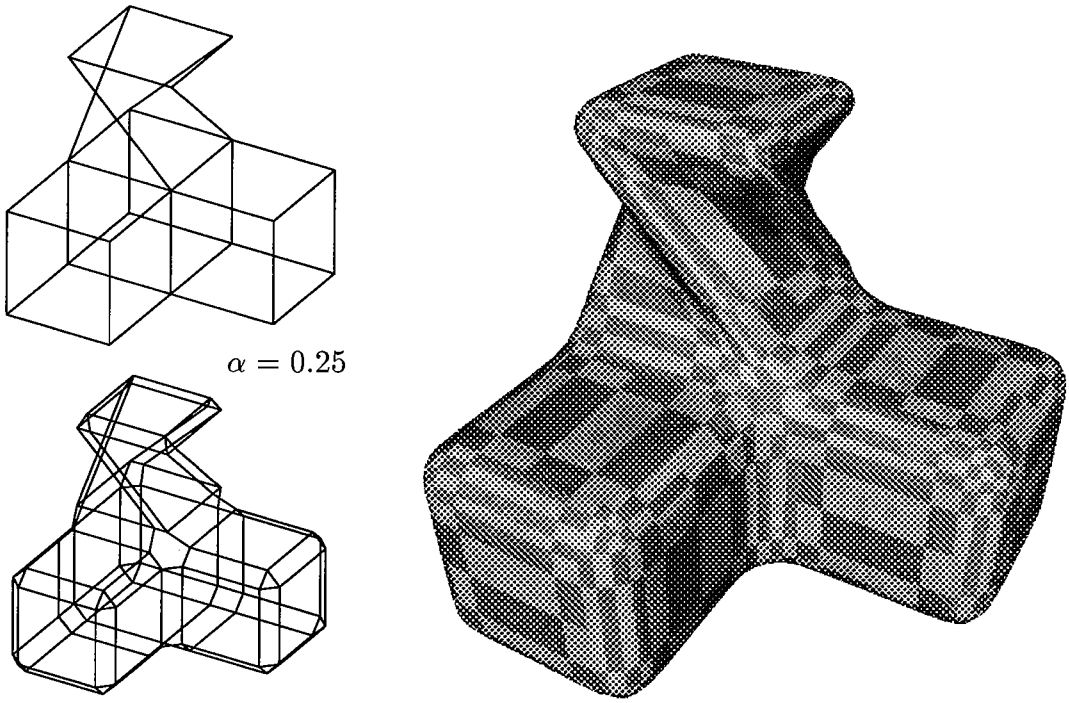

Figure 1.1(a): Blended cubes with a twist.

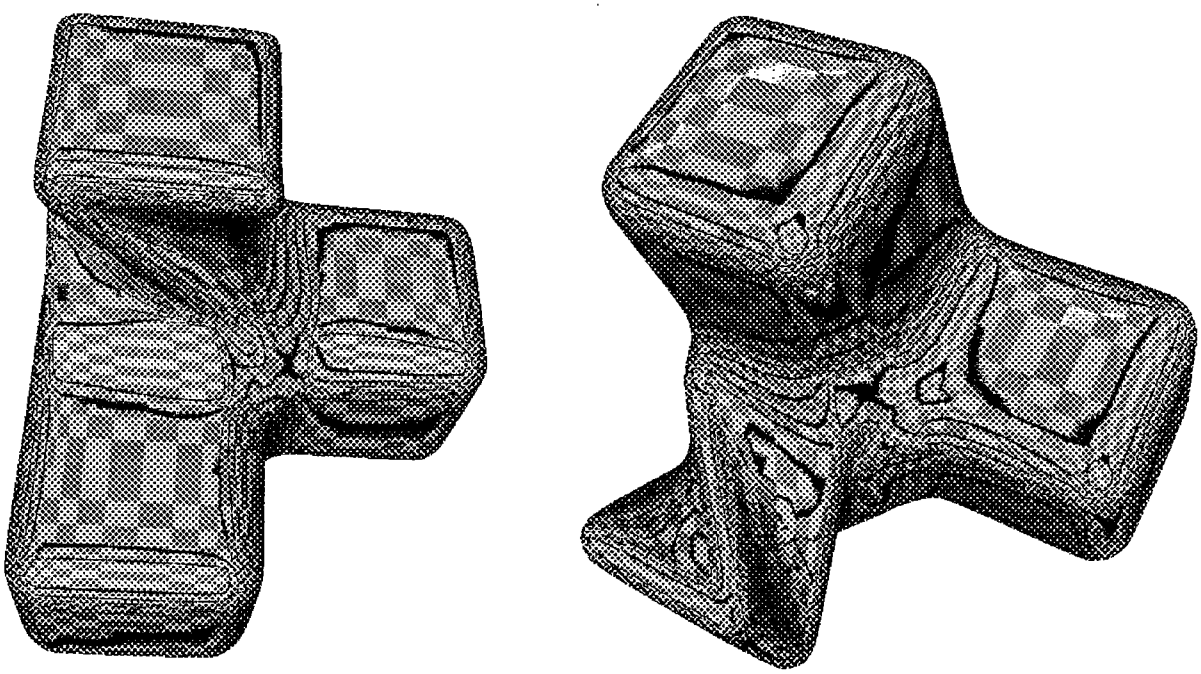

Figure 1.1(b,c): Reflection lines (isoclines) on the same object.

bicubic extension beyond the biquadratic spline surface is not parametrically C^1: the reparametrization map is a quadratic perturbation of the identity rather than the identity. This difference is crucial, since it leaves the necessary degrees of freedom for a *local* construction of low degree.

From a discrete, corner cutting point of view, the second stage of the algorithm is

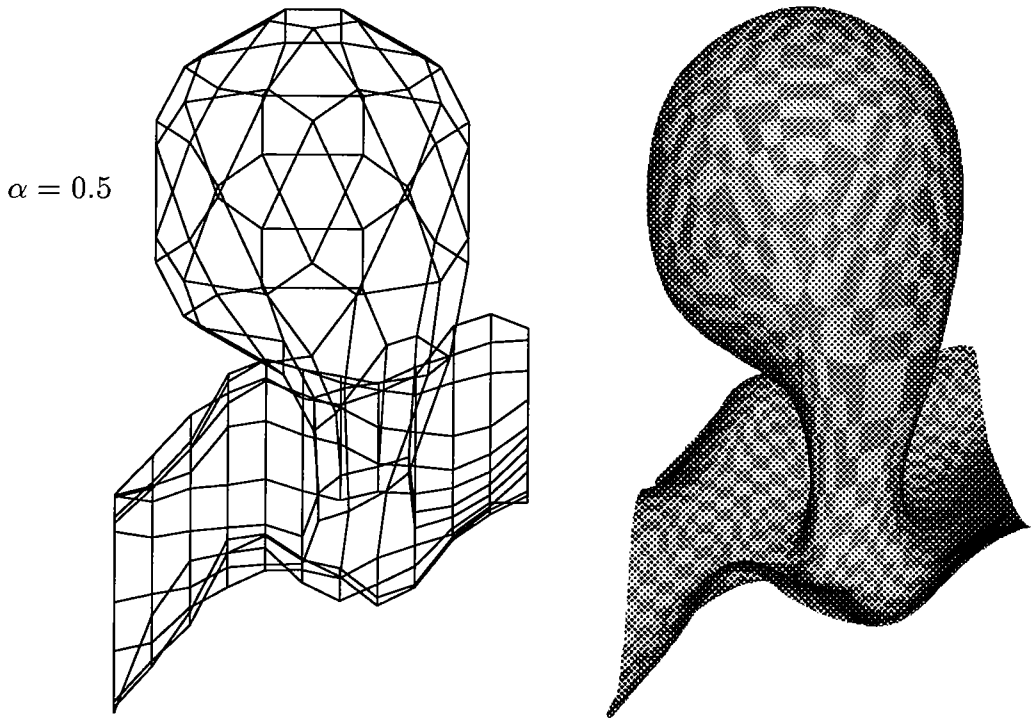

Figure 1.2: A bicubic drop in the sea of biquadratic splines (model of a salt dome).

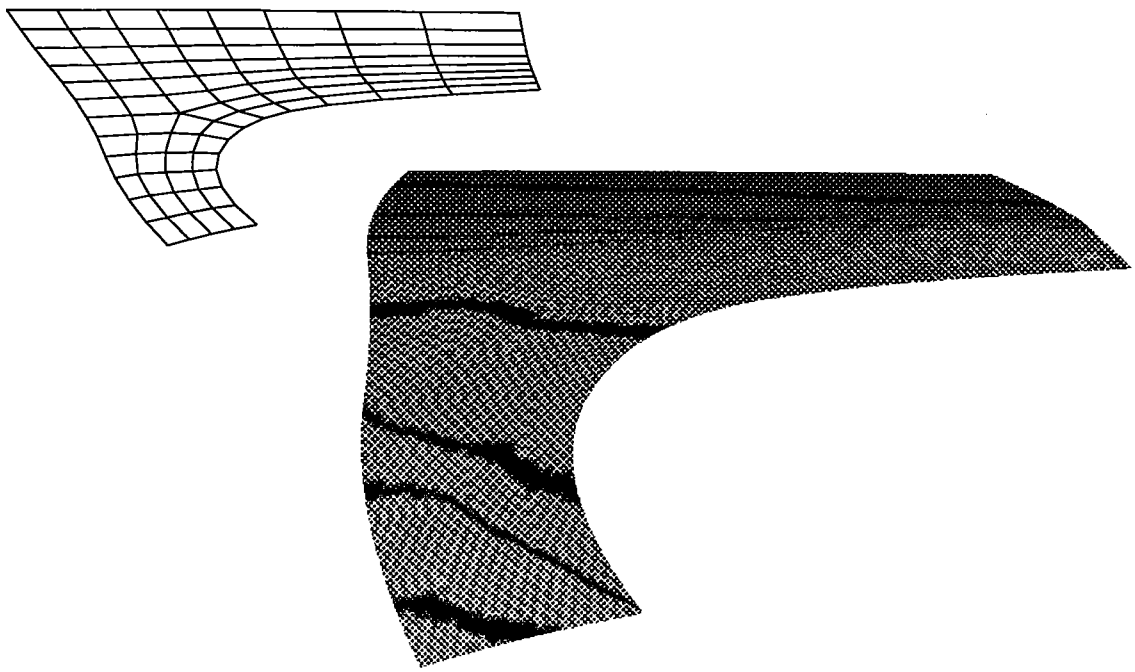

Figure 1.3: A slightly curved car part.

a rule for introducing additional cuts such that a well-known uniform cutting procedure, Chaikin's respectively de Casteljau's algorithm, thereafter will generate a C^1 surface in the limit. This point of view reflects the author's preference to evaluate and display patches in Bernstein-Bézier form by subdivision aka recursive application of de Casteljau's algorithm.

Since it can be guaranteed that the resulting surface interpolates the average of the control points of each original mesh cell, a simple modification to the algorithm interpolates the vertices of the input mesh. Similarly, it is possible to prescribe normals at the vertices. There are no restrictions on the valence of the vertices and in particular none that depend on the parity of the number of adjacent cell edges or neighboring mesh points as in [van Wijk '86].

An example of the proposed construction is the blending of four cubes shown in Figure 1.1. The top cube is twisted to make sure that the 6-sided mesh cell at the common point of the cubes is not symmetric. The object also features irregular 3, 4 and 5-sided mesh cells. The second example, Figure 1.3, models the discretely sampled (zero) level set of a trivariate map. The third shows approximate reflection lines on a slightly curved surface. Note the absence of loops, especially in the reflection line across the 5-valent vertex. To display the objects and the reflection lines, Gouraud shading based on points and normals on the surfaces is used.

Section 2 details the 3-stage construction: (1) an initial corner cutting to give the object its rough shape and curvature, (2) the interpretation of the quadrilateral, 4-valent portion of the refined mesh as a (rational) B-spline control mesh, (3) the tangent-plane continuous cover of the remaining holes in the B-spline complex via the quadratic reparametrizations

$$\phi_i(t_1,t_2) := \mathrm{id} + t_1 t_2 \begin{bmatrix} a_i \\ a_{i-1}(1-t_2) \end{bmatrix}, \quad \text{and} \quad \psi_i(t_1,t_2) := \mathrm{id} + t_1(1-t_2) \begin{bmatrix} 2c \\ 0 \end{bmatrix}.$$

Section 3 establishes the consistency and continuity of the resulting surface and proves some simple shape properties.

2. The G^1 construction in analytic, Bézier and control point representation

Denote by G^1 the agreement of the derivatives of two maps p and q from $\mathbb{R}^2$ to $\mathbb{R}^n$ after reparametrization by a map φ from $\mathbb{R}^2$ to $\mathbb{R}^2$ that connects the domains Ω_p and Ω_q of p and q. That is, the algorithm constructs a surface that has a local, but not necessarily a global C^1 parametrization by enforcing

$$D_1 p_{|E_p} = D_1(q \circ \varphi)_{|E_p},$$

where $\varphi(E_p) = E_q$, E_p and E_q are edges of Ω_p and Ω_q respectively, D_1 denotes differentiation in the direction perpendicular to E_p and φ maps interior points of Ω_q to exterior points of Ω_p to avoid cusps. The components of φ are $\varphi^{[1]}$ and $\varphi^{[2]}$

The algorithm is explained in three equivalent representations: in the above analytic representation that focuses on the connecting map φ, in Bernstein-Bézier (BB) representation and as a corner cutting process that computes new points as averages of old ones

via a (convolution) mask. Figure 2.4 labels the connecting-maps ϕ_i and ψ_i, the patches p_i, $q_{i,j}$ with BB coefficients $P_{jk,i}$ and $Q_{jk,i}$, and the control mesh points A_i, B_{ij}, C_i. To simplify the computation of the product of polynomials in BB form, the binomial factor is combined with the BB coefficient:

$$[b_0,\ldots,b_d] \quad \text{represents} \quad p: t \mapsto \sum_{j=0}^{d} t^j (1-t)^{d-j} b_j$$

so that $[b_0,\ldots,b_d][c_0,\ldots,c_e] = [b_0c_0,\ldots,\sum_{k+l=j} b_k c_l,\ldots,b_d c_e]$. Important constants are: $s \in \mathbb{Z}^+$, the valence of a vertex,

$$c := \cos(\frac{2\pi}{s}) \quad \text{and} \quad a := \frac{c}{1-c}.$$

With this notation, we can now state the basic algorithm. The end of the section specifies two simple extensions of the algorithm that guarantee interpolation of the mesh vertices and allow for conic blends and, more generally, for rational patches in the surface.

The Algorithm: Steps A1-A3

Input: an open or closed bivariate mesh of arbitrary genus and connectedness.

Output: (the specification of) a tangent-plane continuous surface consisting of biquadratic and bicubic patches. The surface interpolates the centroids of the input mesh cells.

Shape parameters:
(a) For each mesh cell f of the input mesh a cut ratio $0 < \alpha_f < 1$ can be specified. The size of the tangent plane at the center S of f decreases, resp. increases with α_f. The default, $\alpha_f = 0.5$ distributes the curvature most evenly across the edge between two faces. Smaller values for both faces increase and larger values decrease the curvature across the edge.
(b) For every non quadrilateral cell f of the refined mesh, there is a scalar $\beta_f \geq 0$ that measures the distance of the interpolation point from the centroid of that mesh cell. The default is $\beta_f = 0$.

(A1) Refinement of the mesh. In two steps, a refined mesh of *control points* is created from the input mesh. The refinement coarsely shapes the object by cutting off corners and edges (cf. Figure 2.1). As illustrated by the figure, at each step, s new points are created for each s-sided cell. Each new point connects to new points arising from the two adjacent vertices of the same cell and the two adjacent cells of the same vertex. The new point corresponding to a vertex V of the cell f with centroid F has the location $(1-\alpha_f)V + \alpha_f F$. In Figure 1.1, $\alpha_f = 1/4$ uniformly, while a uniform $\alpha_f = 1/2$ in Figure 1.3 results in more rounded features. In the second step, the ratio of a cell can be obtained as the average of the ratios of the old cells that contribute a vertex. The cutting also isolates non quadrilateral mesh cells so that, with the labels of Figure 2.4, (1) a connected

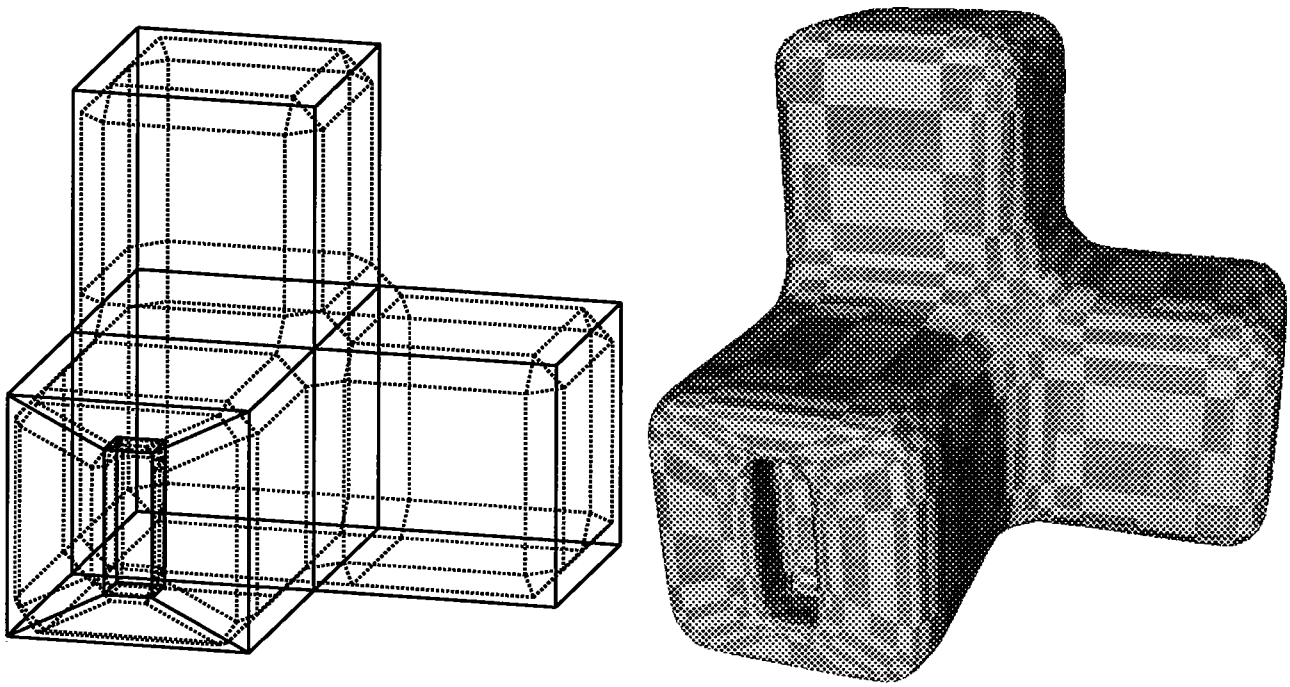

Figure 2.1: Corner cutting for coarse shaping. A slot feature (8 additional points) is added to the smoothed cubes.

biquadratic complex of patches q_{ij}, corresponding to the dark area in Figure 2.3, can be created in Step A2, (2) the control points $B_{i,j}$ in Figure 2.4can be changed without loss of the centroid interpolation property: continuity requires that for every cell of the control mesh with $s \in I := \{i : i = 2m, m \geq 3\} = \{6, 8, 10, ..\}$ edges, the control points labeled $B_{i,j}$ are replaced by $B_{i,j} + (-1)^{i+j}E$, where $E := \frac{-1}{2s} \sum_{i=1}^{s} \sum_{j=1}^{2} (-1)^{i+j} B_{i,j}$. (If a cell of the input mesh has $s \in I$ edges and a vertex with $s' \in I$ neighbors, e.g. a hexagon with a 6-valent vertex, then the shared B_{ij} is fixed the second time.)

Remark: If $\alpha_f = 1/2$ uniformly, the cells of the refined quadrilateral mesh correspond to the same quadratic and can be stored more efficiently (cf. [Doo '78 p 163]).

(A2) The construction of the biquadratic tensor product mesh. Any rectilinear submesh of the refined mesh can be interpreted as the control mesh of a biquadratic tensor product spline surface. Around any s-sided mesh cell this creates a parametrically C^1 biquadratic complex of $2s$ patches $q_{i,j}$, $i = 1..s$, $j = 1, 2$ as sketched by the grey areas in Figures 2.3 and 2.4. That is, $\varphi = \mathrm{id}$ and for adjacent patches q_1 and q_2,

$$D_1 q_1 = D_1 q_2.$$

- *BB representation:* For each quadrilateral mesh cell, the centroid is the vertex coefficient

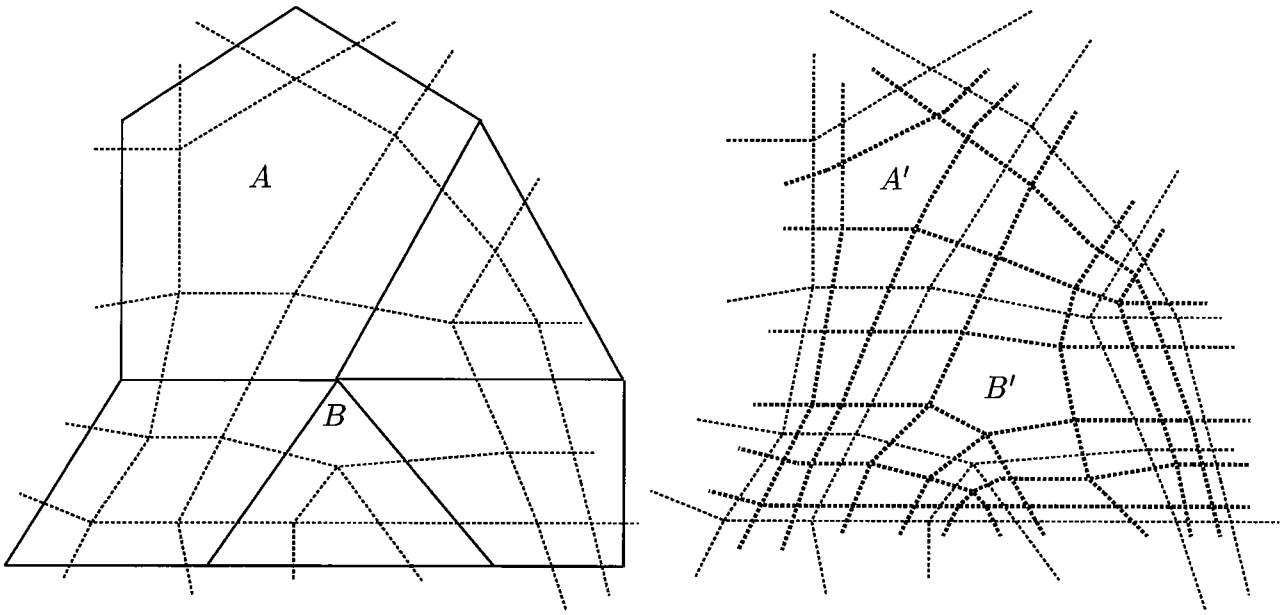

Figure 2.2: A schematic view of 2 steps of the corner cutting algorithm. The input mesh is solid, the first and second refinement are dotted and dashed respectively. Note that both 5-sided cells and vertices with 5 neighbors result in 5-sided cells of the refined mesh.

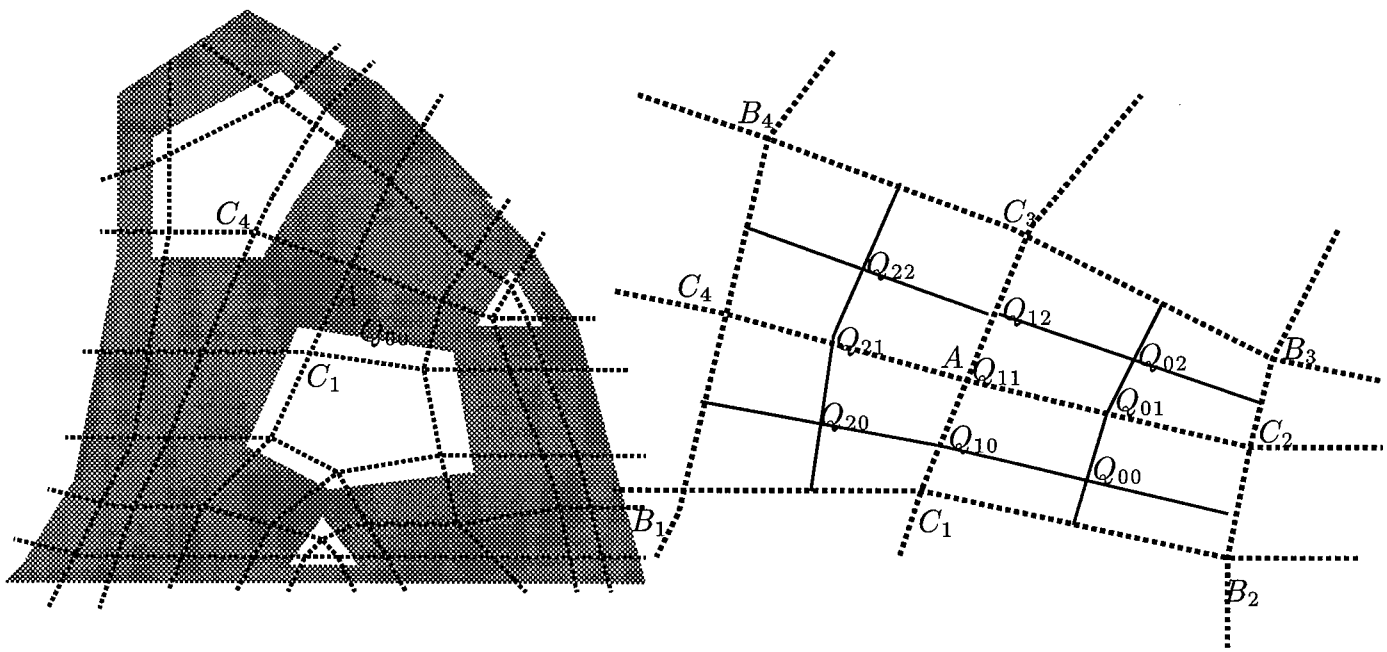

Figure 2.3: Constructing the BB representation of the biquadratic tensor-product mesh dual to the 4-sided mesh cells to cover the grey regions of the refined mesh.

of four BB patches, the average of two adjacent mesh points is the middle coefficient of a quadratic boundary curve of two patches and the mesh points themselves are the respective central coefficients. In Figure 2.3, the quadrilateral $C_1B_2C_2A$ yields $Q_{00} =$

$(C_1+B_2+C_2+A)/4$, $Q_{01} = (A+C_2)/2$, and $Q_{11} = A$. Note the duality of the quadrilateral mesh and the mesh of boundary curves.

In Figure 2.4, the mesh cell $A_iB_{i,1}C_iB_{i,2}$ yields $L_i = Q_{00} = (A_i + B_{i,1} + C_i + B_{i,2})/4$, $Q_{01} = (C_i+B_{i,2})/2$ and $Q_{11} = B_{i,2}$ for the coefficients Q_{ab} of $q_{i,2}$. Note that all coefficients computed are in the grey area outside the pentagon.

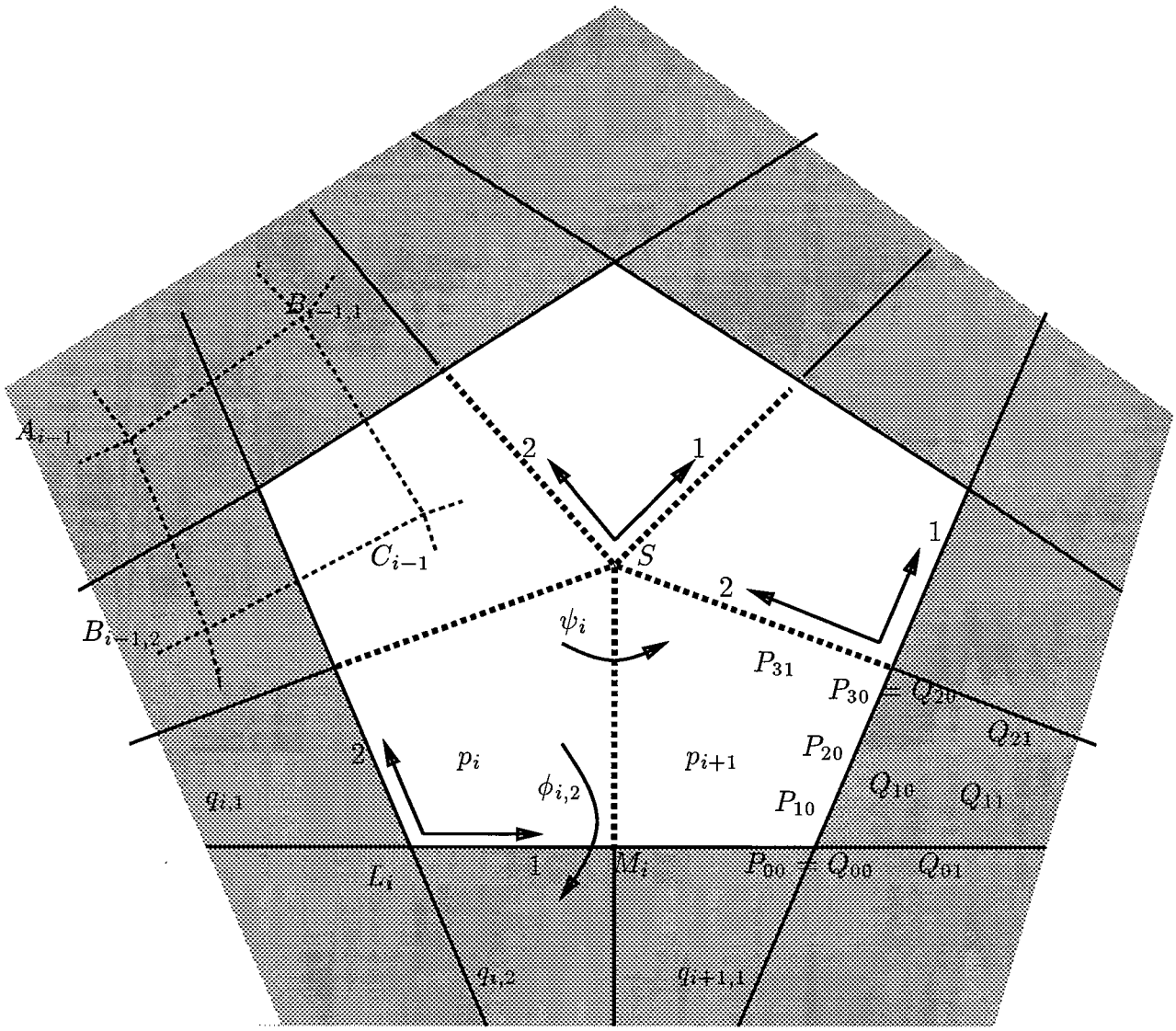

Figure 2.4: A schematic view of the patches in the vicinity of a non quadrilateral mesh cell. For construction and proof, it is convenient to coordinatize p_i with respect to three different domain corners. The curved arrows indicate the reparametrization by ϕ and ψ.

(A3a) Extension of the tangent plane across the spline complex. Each patch $q_{i,j}$ of the complex is extended across the boundary of the complex by choosing the patches p_i

so that along the common boundary $p_i(E_j) = q_{i,j}(\phi_{i,j}(E_j))$,

$$D_j p_i = D_j(q_{i,j} \circ \phi_{i,j}), \tag{C}$$

where $a_i = a := \frac{c}{1-c}$ for now and

$$\phi_{i,1} := \mathrm{id} + t_1 t_2 \begin{bmatrix} a_i \\ a_{i-1}(1-t_2) \end{bmatrix}, \qquad \phi_{i,2} := \mathrm{id} + t_1 t_2 \begin{bmatrix} a_{i-1}(1-t_1) \\ a_i \end{bmatrix}$$

in the coordinate system of the domain of p_i at L_i. The coordinate system is oriented as in Figure 2.4: $(t_1, 0) = E_2$, $p(0,0) = L_i$, $p(1,0) = M_i$. Geometrically, the constraint is at L_i that $D_j p_i = D_j q_{i,j}$ and at M_i that $D_j p_i$ and $D_j q_{i,j}$ are collinear. In between, the tangent direction varies quadratically in contrast to a parametrically C^1 extension across the boundary of the complex.

• *BB representation:* The coefficients P_{j0}, $j = 0..3$ are obtained from the coefficients Q_{l0}, $l = 0..2$ by degree raising, i.e.

$$[P_{00}, 3P_{10}, 3P_{20}, P_{03}] = [1,1][Q_{00}, 2Q_{10}, Q_{02}].$$

Due to degree raising, the transversal BB differences of the patch complex have to be scaled by 2/3, so that the 4 constraints on P_{j1}, $j = 0..3$ across the edge $L_i M_i$ read

$$[P_{01} - P_{00}, 3(P_{11} - P_{10}), 3(P_{21} - P_{20}), P_{31} - P_{30}]$$

$$= -[1, 1+a] * \frac{2}{3}[Q_{01} - Q_{00}, 2(Q_{11} - Q_{10}), Q_{21} - Q_{20}] + [0, a, 0] * [Q_{10} - Q_{00}, Q_{20} - Q_{10}].$$

The first constraint, $P_{01} = P_{00} + \frac{2}{3}(Q_{00} - Q_{01})$, holds after raising the degree of the quadratic boundary curve.

• *control point representation:* The BB coefficients can be expressed in terms of the control points via the following "masks":

$$P_{00,i} = \frac{1}{4}(B_{i,2} + B_{i,1} + C_i + A_i), \qquad P_{10,i} = \frac{1}{12}(5B_{i,2} + B_{i,1} + 5C_i + A_i),$$

$$P_{20,i} = \frac{1}{12}(5B_{i,2} + B_{i+1,1} + 5C_i + C_{i+1}), \qquad P_{30,i} = \frac{1}{4}(B_{i,2} + B_{i+1,1} + C_i + C_{i+1}).$$

$$P_{11,i} = \frac{1}{36}(5B_{i,2} + 5B_{i,1} + A_i + 25C_i) + \frac{a}{36}(B_{i,2} - B_{i,1} + 5C_i - 5A_i)$$

$$P_{21,i} = \frac{1}{36}(5B_{i,2} + 5C_{i+1} + B_{i+1,1} + 25C_i) + \frac{a}{36}(-11B_{i,2} + 3B_{i+1,1} + 3C_{i+1} + 5C_i)$$

$$P_{31,i} = \frac{1}{12}(B_{i,2} + B_{i+1,1} + 5C_{i+1} + 5C_i) + \frac{a}{6}(C_{i+1} + C_i - B_{i,2} - B_{i+1,1})$$

Remark: If $a = 0$, then the coefficients correspond to those of a degree-raised quadratic.

(A3b) Smooth covering of the interior of non quadrilateral mesh cells. The constants $a_i = a$ of the connecting-maps ϕ_i in the tangent extension were chosen so that tangent plane continuity across the interior boundaries can be enforced as

$$D_1 p_{i-1} = D_1(p_i \circ \psi_i), \quad \text{where} \quad \psi_i := \mathrm{id} + t_1(1-t_2)\begin{bmatrix} 2c \\ 0 \end{bmatrix}, \tag{I}$$

where $c := \cos(\frac{2\pi}{s})$, D_1 is the derivative across the joint boundary of the patches and $p_i(0,0) = S$, i.e. we use the coordinate system at S in Figure 2.4.

• *BB representation:* Constraint C of Step 2 fixes all but the central vertex S and the adjacent (tangent and twist) coefficients, $P_{23,i} = P_{32,i-1}$, $P_{32,i} = P_{23,i+1}$ and $P_{22,i}$ of the patches p_i. The 4 constraints across the edge M_iS read

$$\begin{aligned}[P_{20,i-1} - P_{30,i-1}, 3(P_{21,i-1} - P_{31,i-1}), 3(P_{22,i-1} - P_{32,i-1}), P_{23,i-1} - P_{33,i-1}] \\ + [P_{02,i} - P_{03,i}, 3(P_{12,i} - P_{13,i}), 3(P_{22,i} - P_{23,i}), P_{32,i} - P_{33,i}] \\ = [0, -2c] * [P_{31,i-1} - P_{30,i-1}, 2(P_{32,i-1} - P_{31,i-1}), P_{33,i-1} - P_{32,i-1}].\end{aligned}$$

Two of these constraints hold already by Step 2.

To determine S, define the averages $S_P := \frac{1}{s}\sum_{i=1}^{s} P_{31,i}$ and $S_C := \frac{1}{s}\sum_{i=1}^{s} C_i$. If there exists a convex triangulation of the mesh (in the vicinity of the s-sided mesh cell and not including the cell), then one can define $\beta^* \geq 1$ to be the smallest value such that $S_C + \beta^*(S_P - S_C)$ intersects the interior cone formed by the planar extension of the triangles. Otherwise set $\beta^* = 1$. Then

$$S = S_C + \beta(S_P - S_C), \quad 0 \leq \beta \leq \beta^*. \tag{2.5}$$

guarantees interpolation at the centroid if $\beta = 0$ and allows for a convex construction if $\beta^* > 1$ and $\beta \geq 1$.

Since $P_{33,i} = S$ and $P_{23,i} = P_{32,i-1}$, the remaining constraints are

$$2(1-c)S = P_{32,i-1} - 2cP_{32,i} + P_{32,i+1} \tag{I$_3$}$$

$$2((1-c)P_{32,i} + cP_{31,i}) = P_{22,i-1} + P_{22,i}. \tag{I$_4$}$$

There are three degrees of freedom that allow for a number of approaches. We choose an explicit symmetric construction below, but point out that it is always possible to solve the least squares problem

$$\min \sum_{i=1}^{s} \|P^*_{32,i} - P_{32,i}\|^2 + \sum_{i=1}^{s} \|P^*_{22,i} - P_{22,i}\|^2 \tag{2.6}$$

subject to the constraints I_3 and I_4, where the $P^*_{32,i}$, $P^*_{22,i}$ are desirable locations for the tangent and twist coefficients (e.g. locations obtained from degree-raising). An explicit

symmetric solution to the constraints subject to the shape parameter α and the choice of S is:

$$P_{32,i} = S + \frac{\alpha}{s}\sum_{l=1}^{s}\cos(\frac{2\pi}{s}l)P_{31,i+l}, \quad 0 < \alpha < 1.$$

The scalar α is a shape parameter proportional to the diameter of the tangent plane of first differences (cf. [Loop '90 Fig.3]) and therefore similar to the corner cutting ratio of the Doo-Sabin algorithm. Define $E_i := (1-c)P_{32,i} + cP_{31,i}$. If $s > 4$, then $0 < c < 1$ and hence E_i is a convex average of the interior coefficients of the boundary curve. The twist are

$$P_{22,i} = \begin{cases} -\sum_{j=1}^{s}(-1)^j E_{i+j} & \text{if } s \text{ is odd} \\ \frac{-2}{s}\sum_{j=1}^{s}(s-j)(-1)^j E_{i+j} & \text{if } s \text{ is even.} \end{cases}$$

- *control point representation:*

$$P_{32,i} = S + \frac{\alpha}{s}\sum_{l=1}^{s}\cos(\frac{2\pi}{s}l)\frac{1-2a}{12}(B_{i+l,2} + B_{i+l+1,1}) + \frac{5+2a}{6}\cos(\frac{\pi}{s})\cos(\frac{2\pi(l+\frac{1}{2})}{s})C_{i+l},$$

$$P_{22,i} = \begin{cases} (1-c)S - \left((1-c)\frac{\alpha}{s} + c\right)\frac{1-2a}{12}E + \frac{5+2a}{6}C_i & \text{odd} \\ (1-c)S + \frac{-2c}{s}\sum_{j=1}^{s}(-1)^j\left((s-j)\frac{1-2a}{12}(B_{i+j,2} + B_{i+j+1,1}) + \frac{5+2a}{12}C_{i+j}\right) & \text{even} \end{cases}$$

Two Extensions of the Algorithm:

(A0) Interpolation at the vertices of the input mesh Do one refinement as in Step A1 and next, for each vertex S of the input mesh, move the control points C_i, $i = 1..s$ whose construction involves S by $S - \frac{1}{s}\sum_{i=1}^{s} C_i$. Then S is the centroid of the resulting cell and will be interpolated. Similarly, one can interpolate normals at the vertices.

(A2a) Conic blends and rational patches To obtain conic blends and, more generally, rational surfaces, treat the control points as vectors in $\mathbb{R}^4$ and the fourth coordinate as an additional shape parameter. If $P, Q : [0..1]^2 \mapsto \mathbb{R}^3$ and $p, q : [0..1]^2 \mapsto \mathbb{R}$ and $P = Q$ and $p = q$ along a boundary shared by the functions P/p and Q/q, then

$$D_1(\frac{Q}{q} \circ \phi) = D_1\frac{P}{p} \qquad \Longleftrightarrow$$

$$q(D_1P - D_1QD_1\phi^{[1]} - D_2QD_1\phi^{[2]}) = Q(D_1p - D_1qD_1\phi^{[1]} - D_2qD_1\phi^{[2]})$$

along that boundary. The latter holds if the masks of the algorithm are applied to the coefficients of $(P, p) \in \mathbb{R}^4$. That is, the fourth coordinate corresponds to the rational weight function. For example, choosing the weight component of two neighboring control points

in the regular mesh to be 3 rather than 1 (and keeping the other weight components at 1) yields two circular arcs with weights (112) and one conic with weights (232). in between:

weights of the control points	1		1		3		1	1
weights of three quadratic boundary curves		1	1	2	3	2	1	1
weights of the control points	1		1		3		1	1

In general, the algorithm works for constructing bivariate surfaces in $\mathbb{R}^n$.

3. Consistency and continuity of the resulting surface

This section proves the correctness of the construction. The first part examines the initial cutting process, the second proves consistency of the construction and smoothness of the surface at L_i, M_i and S respectively and the third discusses the shape of the resulting surface.

3a. The mesh refinement

Denote as type 1 every pair of non-4-sided cells arising from two adjacent non-4-sided cells or from two adjacent non-4-valent vertices and as type 2 every pair of non-4-sided cells arising from a non-4-sided cell and its non-4-valent vertex.

(3.1) Lemma. *The two cuts in Step A1 result in a control mesh such that (R1) every interior control point has four neighbors, (R2) every type 1 pair is separated by three layers of quadrilateral cells and (R3) every type 2 pair is separated by one layer of quadrilateral cells.*

Proof Since every new control point is connected to two new points on the same original cell and across to edges of that cell, R1 holds after the first step. After one step any two cells are separated by one layer of quadrilateral cells. This implies R2. Since every type 2 pair still has a common vertex after one step, R3 follows from the same argument. ■

(3.2) Corollary. *The control points $B_{i,j}$ of a type 1 pair of cells are distinct. The perturbation of any $B_{i,j}$ does not alter the control points of a cell that contains the centroid of a cell of the input mesh.*

The perturbation is motivated by the construction at S, Lemma 3.8. It is the minimal perturbation that enforces $E := \sum_{i=1}^{s}\sum_{j=1}^{2}(-1)^{i+j}B_{i,j} = 0$. The corner cutting process is a variant of the Doo-Sabin algorithm [Doo '78] that preserves some edge directions.

(3.3) Lemma. *The cutting in Step A1 leaves all facet-cell edges parallel to the original facet cells and hence two of the edge-cell edges parallel to original edges.*

Proof The endpoints of the new and old edges together with the centroid form similar triangles. ■

3b. Continuity

To avoid listing a large number of equations, the following proofs are formulated independent of the surface representation as far as possible.

(3.4) Lemma. *The construction in Step A2 yields a parametrically C^1 surface.*

Proof The centroid of four points A, B, C, D in $\mathbb{R}^3$ is also the intersection of the two lines $\frac{A+B}{2}\frac{C+D}{2}$ and $\frac{A+D}{2}\frac{C+B}{2}$. Thus the vertex coefficient Q_{00} is well defined and the tangent coefficients Q_{01} etc. of the patches abutting at Q_{00} lie in the same plane. Since the tangent coefficients are also the average of the central coefficients of adjacent patches, the difference vectors across any boundary agree pairwise. ■

(3.5) Lemma. *Consider a particular corner vertex $L_i = L$ (and therefore drop the subscript i). At L*

$$D_1D_2(q_1 \circ \phi_1) = D_1D_2p = D_1D_2(q_2 \circ \phi_2) \tag{3.6}$$

that is, that the extensions of the patches q_1 and q_2 define the mixed derivative of p consistently.

Proof Expanding the left hand side of Equation 3.6 according to the chain rule and noting that $D_2\phi_{i,1|0} = (0,1)$ and $D_1\phi_{i,2|0} = (1,0)$ we have at 0 (in the coordinate system at L of Figure 2.4)

$$D_1D_2q_1 + D_1q_1D_1D_2\phi_1^{[1]} + D_2q_1D_1D_2\phi_1^{[2]} = D_1D_2q_1 + a_1D_1q_1 + a_2D_2q_1.$$

and similarly $D_1D_2q_2 + a_2D_1q_2 + a_1D_2q_2$ for the right hand side. By construction of the complex, $D_1D_2q_j = -4(B_j - \frac{B_j+C}{2} - \frac{A+B_j}{2} + \frac{A+B_j+B_i+C}{4}) = A + C - B_j - B_i$. Since by construction also $D_jq_2 = D_jq_1$, the left hand side of Equation 3.6 equals the right hand side and uniqueness of the mixed derivative D_1D_2p follows. ■

(3.7) Lemma. *The continuity constraints (I) at $M_i = M$ are consistent with the construction of the tangents across the boundary of the complex.*

Proof Move the coordinate systems of ψ_i, $\phi_{i-1,2}$ and $\phi_{i,1}$ to M_i as in Figure 2.4 to obtain the reparametrizations ψ_i', and $\phi_{i-1,2}' = \phi_{i,1}'$. Thus the inverse image of S is both $\psi_i(0,0) = \psi_i'(0,1)$. Algebraically, one obtains ψ_i' from ψ_i by replacing $1 - t_2$ by t_2, i.e.

$$\psi_i' := \mathrm{id} + t_1t_2 \begin{bmatrix} -2c \\ 0 \end{bmatrix}$$

and similarly

$$\phi_{i-1,2}'(-t_1,t_2) = \phi_{i,1}'(t_1,t_2) = \mathrm{id} + at_2(1-t_1) \begin{bmatrix} t_1 \\ -1 \end{bmatrix}.$$

We need to check that along the common boundary and in particular at M that

$$D_1^m p_{i-1|(0,t_2)} = D_1^m(p_i \circ \psi_i')_{|(0,t_2)}, \quad m = 0,1.$$

Clearly at $(0,0)$, $p_{i-1} = p_i \circ \psi_i'$, $D2p_{i-1} = (1+a)D_2q_{i-1,2} = (1+a)D_2q_{i,1} = D_2(p_i \circ \psi_i')$, and

$$D_1p_{i-1} = D_1q_{i-1,2} = D_1q_{i,1} = D_1p_i = D_1(p_i \circ \psi_i').$$

To show that also $D_2D_1p_i = D_2D_1(p_i \circ \psi_i')$, we observe that $D_1D_2q_{i-1,2} = D_1D_2q_{i,1}$, $D_1q_{i-1,2} = D_1q_{i,1}$ and hence

$$\begin{aligned} D_2D_1(q_{i-1,2} \circ \phi_{i-1,2}') &= -D_2D_{-1}(q_{i-1,2} \circ \phi_{i-1,2}') \\ &= (1+a)D_1D_2q_{i-1,2} + a(D_1q_{i-1,2} + D_2q_{i-1,2}) \\ &= D_2D_1(q_{i,1} \circ \phi_{i,1}') + 2aD_2q_{i,1} \end{aligned}$$

This implies the fourth equality below, while the other equalities follow from the definition of p_i and p_{i-1} and the connecting maps.

$$\begin{aligned} D_2D_1p_i - 2cD_1p_i = D_2D_1(p_i \circ \psi_i') = D_2D_1p_{i-1} &= D_2D_1(q_{i-1,2} \circ \phi_{i-1,2}') \\ = D_2D_1(q_{i,1} \circ \phi_{i,1}') + \frac{2a}{1+a}D_2p_i. \end{aligned}$$

The constraint holds since $-2c = \frac{2a}{1+a}$. ■

(3.8) Lemma. *The choices of the tangent coefficients $P_{32,i}$ and $P_{22,i}$ in Step A3b solve the constraints* I_3 *and* I_4 *and thus enforces consistency at S.*

Proof Constraint I_3 holds since

$$\begin{aligned} &\sum_{i=1}^{s} \cos(\frac{2\pi}{s}i)(P_{31,i-1} - 2cP_{31,i} + P_{31,i+1}) \\ &= \sum_{i=1}^{s} P_{31,i}\big(\cos(\frac{2\pi}{s}(i-1)) + \cos(\frac{2\pi}{s}(i+1)) - 2\cos(\frac{2\pi}{s})\cos(\frac{2\pi}{s}i)\big) = 0. \end{aligned}$$

If s is odd, then

$$P_{22,i-1} + P_{22,i} = -\sum_{j=1}^{s}(-1)^j(E_{i+j-1} + E_{i+j}) = 2E_i$$

as required. If s is even, then

$$\sum_{j=1}^{s}(-1)^jP_{32,j} = \frac{\alpha}{s}\sum_{j=1}^{s}(-1)^j\sum_{l=1}^{s}\cos(\frac{2\pi}{s}l)P_{31,j+l} = 0$$

since $\sum_{j=1}^{s}(-1)^j\cos(\frac{2\pi}{s}j) = 0$ and $\sum_{j=1}^{s}(-1)^jP_{31,j} = 0$ since the C_i cancel and the perturbation forces $E := \sum_{i=1}^{s}\sum_{j=1}^{2}(-1)^{i+j}B_{i,j} = 0$. ($E = 0$ is also a necessary constraint for solvability.) Therefore $\sum_{j=1}^{s}(-1)^jE_j = 0$ and

$$P_{22,i-1} + P_{22,i} = \frac{-2}{s}\sum_{j=1}^{s}(s-j)(-1)^j(E_{i+j-1} + E_{i+j}) = \frac{-2}{s}\big(\sum_{j=1}^{s}(-1)^jE_j - sE_i\big) = 2E_i$$

as required. ■

3c. Shape considerations

Consider a cone made from n similar triangles meeting at an apex. If the cutting ratios are alternatingly high and low, say 0.25 and 0.5, then the n-cell resulting from the cutting process has a boundary in the form of a crown. This illustrates that e.g. convexity preservation depends crucially on the cutting ratios. Nevertheless, a few statements can be made, since the averaging operation in Step A2 is just a change of basis from B-spline to BB form representation so that the shape of the biquadratic surface already follows from the control mesh.

(3.9) Lemma. *If four cells surround a vertex A, then the biquadratic patch with center coefficient $Q_{11} = A$ has zero curvature if and only if the cells are coplanar. Two adjacent coplanar cells, give rise to a linear boundary curve.*

Proof The 9 by 9 system of equations relating the control points to the BB coefficients is of full rank. While the linearity of the boundary curve follows from coplanarity, the reverse does not hold, because the system is 3×6. ■

(3.10) Lemma. *The curvature at S is zero if and only if $P_{31,i}, i = 1..s$ and S lie in the same plane.*

Proof Let $P(n)$ be the normal component of P. According to Lemma 3.8, all $P_{32,i}$ and S lie in the same tangent plane. The normal direction to that plane is $n = A_i \times A_{i+1}$, where $A_i := \sum_{l=1}^{s} \cos(\frac{2\pi}{s} l) P_{31,l+i}$. If some $P_{31,i}$ does not lie in that plane, then (a) the curvature of the ith boundary curve is nonzero and (b) the $P_{22,i}$ do not all lie in the plane either. The latter follows by contradiction from I_4: $2cP_{31,i} = 2((1-c)P_{32,i}(n) + cP_{31,i}(n)) = P_{22,i-1}(n) + P_{22,i}(n) = 0$. Conversely, if all $P_{31,i}$ lie in the tangent plane, then the normal components of all $P_{32,i}$ and $P_{22,i}$ are zero by construction. ■

(3.11) Corollary. *If all C_i and $\frac{1}{2}(B_{i,1} + B_{i,2})$ are in the same plane, then the normal curvatures at S are zero. If additionally all A_i and $\frac{1}{2}(B_{i,1} - B_{i,2})$ are in the common plane, then the bicubic cover is flat.*

Proof Follows directly from the control point representation. ■

While it is desirable that planar data give rise to a planar surface, the choice of S should prevent flatness for convex data. For the following proof concerning a non quadrilateral cell we assume (a) local symmetry of the control mesh, i.e. A_{i+1}, $B_{i+1,j}$ and C_{i+1} can be obtained from A_i, B_{ij} and C_i by a rotion by $\frac{2\pi}{s}$ and (b) local convexity of the control mesh, i.e. the extensions of the cells spanned by A_i, B_{ij} and C_i $i = 1..s$ form a convex cone. If the mesh at a non quadrilateral cell is locally symmetric, then cell with vertices C_i is planar and we may denote the normal distance of a point P from that plane by $P(n)$. Also due to the symmetry the subscripts of the control points can be dropped and we have $A(n) < B(n) < C(n) = 0 < \beta = P_{32,i}(n) = S(n)$ if the control mesh is also locally convex.

(3.12) Lemma. *If the control mesh is locally convex and symmetric, then for $s > 4$ the boundary curves are convex if and only if $1 \leq \beta \leq \beta^*$; for $s = 3$, $\beta = 1$ is sufficient. If $s > 4$, then the normal components of the coefficients $P_{ij}(n)$ are monotonically increasing with $i + j$ if and only if $A(n) > \frac{4+8a}{5a-1} B(n)$.*

Proof By symmetry, the curve with coefficients $[P_{30,i}, 3P_{31,i}, 3P_{32,i}, P_{33,i}]$ constructed in Step A3, common to two adjacent bicubic patches lies in a perpendicular plane. By Step A3a and since $1 < a = \frac{1}{1-c}$ for $s > 4$, and $B(n) < 0$,

$$\begin{aligned} P_{31,i}(n) &= \frac{C_{i+1}(n) + C_i(n)}{2} + \frac{2a-1}{12}(C_{i+1}(n) + C_i(n) - B_{i,2}(n) - B_{i+1,1}(n)) \\ &= \frac{1-2a}{6} B(n) > 0. \end{aligned}$$

That is, the plane through the C_i separates the M_i from the plane in which S and the coefficients $P_{32,i}$ lie if $S = S_C$. The boundary cubic has therefore an inflection in the BB polygon and hence in the curve if and only if $\beta \geq 1$, i.e. $S(n) \geq P_{31,i}(n)$.

For $s > 4$, set $A(n) =: kB(n)$, $k > 1$ and $b := \frac{1-2a}{6} < 0$. Since $\beta \geq 1$, $P_{33}(n) = P_{31}(n) + \epsilon b B(n)$, $\epsilon \geq 0$. Then

$$\begin{bmatrix} P_{03} & P_{13} & P_{23} & P_{33} \\ P_{02} & P_{12} & P_{22} & P_{32} \\ P_{01} & P_{11} & P_{21} & P_{31} \\ P_{00} & P_{10} & P_{20} & P_{30} \end{bmatrix} (n) = \begin{bmatrix} \frac{1}{2} & b & (1+\epsilon)b & (1+\epsilon)b \\ \frac{1}{2} & b + \frac{a}{9} & (1+(1-c)\epsilon)b & (1+\epsilon)b \\ \frac{1}{2} + \frac{k}{12} & \frac{10}{36} + \frac{1-5a}{36} k & b + \frac{a}{9} & b \\ \frac{1}{2} + \frac{k}{4} & \frac{1}{2} + \frac{k}{12} & \frac{1}{2} & \frac{1}{2} \end{bmatrix} B(n).$$

We check the four more difficult cases.

$$\begin{aligned} P_{22}(n) < P_{21}(n): &\quad (1-c)\epsilon b < 0 < \frac{a}{9} \\ P_{21}(n) < P_{20}(n): &\quad b + \frac{a}{9} = \frac{3-4a}{18} < 0 < \frac{1}{2} \\ P_{11}(n) < P_{10}(n): &\quad \frac{10 - 18 + k - 3k - 5ak}{36} < -\frac{8+7k}{36} < 0 \\ P_{12}(n) < P_{11}(n): &\quad \frac{6 - 8a - 10 - k + 5ak}{36} < 0 \end{aligned}$$

The last relation is responsible for the extra condition on the normal component of the A_i and B_{ij}. ■

(3.14) Remark on parametric C^1 continuity, bicubic patches and triangular mesh cells.

Choosing the extension across the boundaries of the biquadratic complex to be parametrically C^1, i.e. $\phi_{i,j}$ to be the identity, leads in general to an inconsistent system of equations for bicubics. In particular, $D_2 D_1 \psi_i'^{[1]}(0,0)$ has to be zero rather than $-2c(1-t)$ and therefore $D_1 \psi_i'^{[1]}$ has to be at least quadratic. This implies that s additional constraints have to be enforced but there are only two degrees of freedom in addition to S:

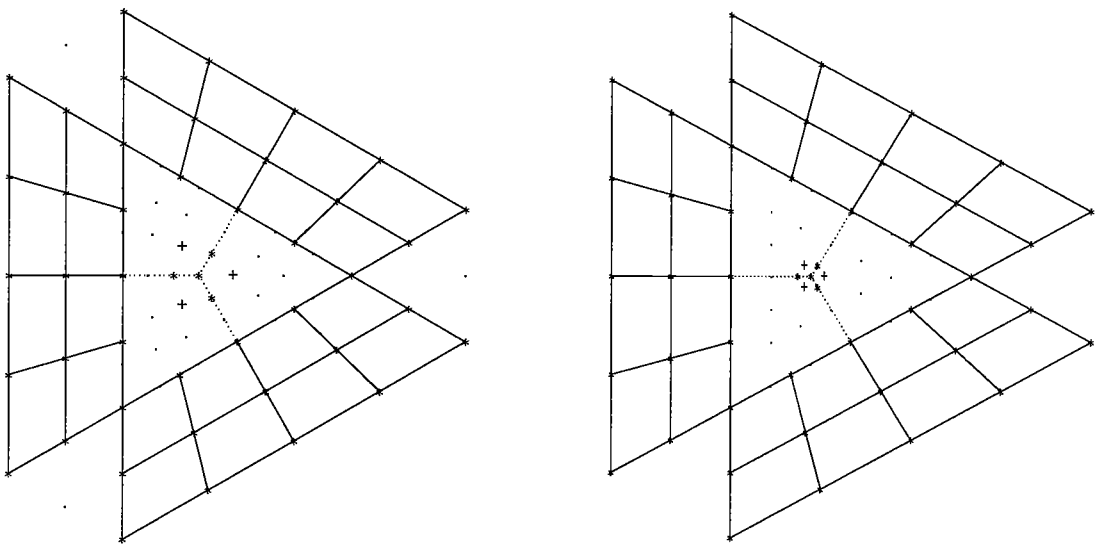

Figure 3.13: Distribution of the BB coefficients for (left) the G^1 join of Section 2 (right) the parametric C^1 join of Remark 3.14.

one tangent coefficient and one twist coefficient may be chosen freely. Therefore, one can in general not cover an s-sided hole with bicubics that extend a biquadratic patch complex parametrically C^1 across its boundary.

An exception occurs for $s = 3$ due to the fact that three points always lie in a plane. We may choose the common boundary curve of two adjacent patches to be degree-raised quadratics. Then, after extending the patch parametrically C^1, one can choose

$$\psi_i := \mathrm{id} + t_1(1-t_2)^2 \begin{bmatrix} 2c \\ 0 \end{bmatrix}$$

i.e. $D_1\psi_i^{'[1]} \sim [0, 0, \frac{2}{3}]$. Thus the mesh cell is smoothly covered by setting $p_{i-1}(0, t_{i-1}) = p_i(0, t_i) \sim [M_i, 2m_i, S]$ (with the coordinate system at M_i),

$$\begin{aligned}
m_i &= \frac{1}{2}(C_i + C_{i+1}) \\
S &= \frac{1}{3}(m_1 + m_2 + m_3) = \frac{1}{3}(C_1 + C_2 + C_3) \\
P_{32,i} &= S + \frac{2}{3}(m_i - S) = \frac{1}{9}(4C_i + 4C_{i+1} + C_{i-1}) \\
P_{22,i} &= \sum_{j=0}^{2}(-1)^j(P_{32,i+j} + \frac{1}{6}(m_i - M_i)) \\
&= \frac{1}{9}(7C_i + C_{i+1} + C_{i-1}) + \frac{1}{6}C_i - \frac{1}{12}\sum_{j=0}^{2}(-1)^j(B_{j,2} + B_{j+1,1}).
\end{aligned}$$

Since $\phi_{i,j}$ is the identity, this solution can also be applied if the surrounding patch complex is bicubic. (This is the construction in [Gregory,Zhou '90, Figs 4.1–3].) Figure 3.15 compares the distribution of the BB coefficients for the two connecting maps.

4. Conclusion

The three steps of the preceding construction combine a number of techniques, some known and some new. Known is the interpretation of the regular mesh as a mesh of control points for a tensor-product spline in Step A2. Also known is the Doo-Sabin type refinement of the input mesh in Step A1 of the algorithm. However, it is used for a new and different purpose. Rather than iterating to the limit, it only serves to give an intuitive handle for distributing curvature on the surface and to separate irregularities in the mesh. Also new is the choice of a quadratic reparametrization to connect the bicubic patches with the biquadratic spline complex in Step A3a. Finally, the explicit solution to the vertex enclosure problem for a non 4-valent vertex in the form of a simple averaging mask for the mixed derivatives is new and should be helpful for similar control mesh based algorithms.

Even though the examples are encouraging, the characterization and proof of the shape properties of the construction is at this point limited to relatively simple cases. The strong points of the algorithm are its low degree, standard tensor-product representation and the simplicity of the construction as an application of masks to control points. It may be interpreted as generating a spline space with additional interpolation properties.

References

A.A. Ball, D.J.T. Storry (1986), A matrix approach to the analysis of recursively generated B-spline surfaces, *Computer Aided Design* **18**, No 8: 437–442.

A.A. Ball, D.J.T. Storry (1988), Conditions for tangent plane continuity over recursively generated B-spline surfaces, *ACM TOG* **7**, No 2: 83–1002.

A.A. Ball, D.J.T. Storry (1989), Design of an n-sided surface patch from Hermite boundary data. *Computer Aided Geometric Design* **6**: 111–120.

E. Catmull, J. Clark (1978), Recursively generated B-spline surfaces on arbitrary topological meshes, *Computer Aided Design* **10**, No 6: 350–355.

D. Doo (1978), A subdivision algorithm for smoothing down irregularly shaped polyhedrons, *Proceedings on interactive techniques in computer aided design*, Bologna: 157–165.

N. Dyn, D. Levin, D. Liu (1992), Interpolatory convexity preserving subdivision schemes for curves and surfaces, preprint.

T.N.T. Goodman (1988), Closed surfaces defined from biquadratic splines, *Report AA 886 University of Dundee.*

J.A. Gregory (1974), Smooth Interpolation without Twist Constraints, *Computer Aided Geometric Design*, 71-88, R.E. Barnhill, R.F. Riesenfeld, eds. , Academic Press.

J.A. Gregory (1990), Smooth parametric surfaces and n-sided patches, *Computation of curves and Surfaces*, W. Dahmen, M. Gasca and C.A. Micchelli, eds., Kluwer Academic Publishers, Dordrecht, 1990: 457–498.

J.A. Gregory, J. Zhou(1990), Filling polygonal holes with bicubic patches, *TR/05/91*, Brunel University,Uxbridge, UB8 3PH, England, March 1991.

J. M. Hahn (1989), Filling polygonal holes with rectangular patches, *Theory and Practice of geometric modeling*, W. Straßer and H.-P. Seidel eds., Springer 1989.

K. Höllig, H. Mögerle (1989), G-splines, *Computer Aided Geometric Design* **7**: 197–207.

C. Loop (1987) Smooth subdivision surfaces based on triangles, Master's thesis, University of Utah.

C. Loop (1990) A G^1 triangular spline surface of arbitrary topology, manuscript, Dept. of CS and Eng., University of Washington, April 1990.

C. Loop, T. DeRose (1990), Generalized B-spline surfaces of arbitrary topology, *Proceedings of Siggraph '90.*

H. Mögerle (1992), *G-splines höherer Ordnung*, thesis, Math Inst A, University of Stuttgart, Germany.

M. Sabin, Non-rectangular surface patches suitable for inclusion in a B-spline surface, in P. ten Hagen (ed.), *Proceedings of Eurographics '83*, North Holland, 1983: 57–69.

R.F. Sarraga (1987), G^1 Interpolation of Generally Unrestricted Cubic Bézier curves, *CAGD* 4(1-2):23–40,1987

J.J. van Wijk (1984), Bicubic patches for approximating non-rectangular control-point meshes, *Computer Aided Geometric Design* **3**, No 1: 1–13.